The slumping of a cohesive granular column: Continuum and discrete modeling

Anaïs Abramian, Lydie Staron, and Pierre-Yves Lagrée

Citation: Journal of Rheology **64**, 1227 (2020); doi: 10.1122/8.0000049
View online: https://doi.org/10.1122/8.0000049
View Table of Contents: https://sor.scitation.org/toc/jor/64/5
Published by the The Society of Rheology

The slumping of a cohesive granular column: Continuum and discrete modeling

Anaïs Abramian,[a] Lydie Staron, and Pierre-Yves Lagrée

Sorbonne Université, CNRS - UMR 7190, Institut Jean Le Rond d'Alembert, F-75005 Paris, France

(Received 10 April 2020; final revision received 11 June 2020; published 3 September 2020)

Abstract

Cohesion forces strongly alter the flow properties of a granular material. To investigate this influence, we focus on a simple configuration: the collapse of a cohesive granular column. To do so, we adopt a numerical approach and implement a peculiar rheology in a Navier–Stokes solver (Basilisk): the so-called $\mu(I)$-rheology, usually used for dry granular materials, supplemented by a yield stress for cohesion. With this approach, we recover the stability of the column, assuming the classical Mohr–Coulomb criterion for failure. We then compare this approach with a code based on contact dynamics, which implies forces at the grain scale: we recover the stability of the column as well. Furthermore, this comparison enables us to estimate the macroscopic yield stress based on the cohesive contacts between grains, which bridges the gap between continuous and discrete approaches of cohesive granular matter. © *2020 The Society of Rheology.*
https://doi.org/10.1122/8.0000049

I. INTRODUCTION

Cohesion forces strongly alter the flow properties of a granular material. Instead of flowing homogeneously, grains aggregate and flow intermittently. In nature, a loss of cohesion in soils can trigger catastrophic landslides [1]. In industrial processes, cohesion sometimes prevent materials, like gypsum or plaster, to flow properly. In worst cases, it can clog and stop the flow during a process chain. Techniques have been devised to characterize these materials and, in particular, determine their "flowability." Although these measurements can be useful to compare two powders or give qualitative properties of the material, they still lack a physical base.

To this end, cohesive forces have been modeled at the grain scale, theoretically and numerically. These cohesion forces can be van der Waals forces [2], electrostatic forces, or induced by capillary bridges [3]. However, it is not an easy task to link these properties to the macroscopic flow of an assembly and, in particular, to the friction coefficient or the yield stress. Recently, Gans *et al.* [4] elaborated a coating agent based on a polymer that enables them to get a stable and reproducible cohesive granular material. Doing so, they linked the force between two grains with the macroscopic rheology of the material.

In the wake of these results, we investigate numerically the link between the rheology of cohesive material and cohesive forces at the grain scale. To do so, we develop two numerical implementations based on different approaches: a continuum approach based on the macroscopic, material scale, and a discrete approach based on the grain scale.

From the macroscopic point of view, we describe the material as a fluid of a peculiar rheology. In the first instance, the $\mu(I)$-rheology is a good candidate as it successfully modeled the flow of dry granular materials [5–7]. According to the latter, the shear stress τ is related to the pressure P through [8–10]

$$|\tau| = \mu(I)P, \tag{1}$$

where $\mu(I)$ is the friction, which can involve the static friction coefficient μ_s, as well as a complex dependence on the shear rate encapsulated by the inertial number I.

To take into account cohesion in the material, we introduce a yield stress τ_c in the rheology such that

$$\tau = \tau_c + \mu(I)P, \tag{2}$$

and then solve the flow with a Navier–Stokes solver (Basilisk) [5].

We compare these simulations with a code based on contact dynamics [11,12], solving the motion of individual grains and giving access to individual grain-scale quantities, such as the forces between grains and the number of cohesive contacts.

In this article, we test our numerical implementations on a simple configuration: a granular column (Fig. 1). This is a challenging test because it covers a large range of flow regimes; meanwhile, its duration is short enough for the simulations. We expect the column to remain stable below a threshold height due to the yield stress induced by cohesion. The column then flows when its initial height H_0 exceeds the threshold value,

$$H_c = \frac{4\,\ell_c}{\sqrt{\mu_s^2 + 1} - \mu_s}, \tag{3}$$

where g is gravity and ℓ_c is a cohesive length defined as

$$\ell_c = \frac{\tau_c}{\rho g}, \tag{4}$$

with ρ being the density of the material.

[a]Author to whom correspondence should be addressed; electronic mail: anaisabramian@gmail.com

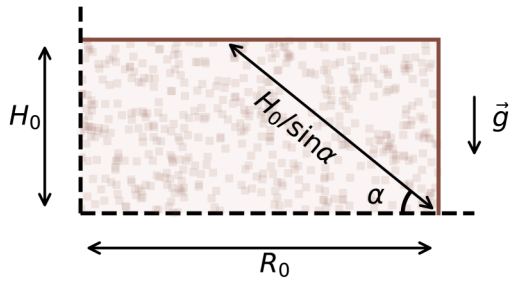

FIG. 1. Two-dimensional cohesive column of height h in a gravity field. At equilibrium, friction μ_s and cohesion τ_c balance the weight of the upper corner along the surface of length $h/\sin\alpha$. This surface of incipient rupture forms an angle α with the horizontal.

Equation (3) is easily shown by considering the upper corner above the column, of mass $M = \rho H_0^2/2\tan\alpha$, sliding with friction μ_s and cohesion τ_c along a slope of angle α (Fig. 1). In this configuration, the initial height of the column rewrites as a function of the fracture angle

$$H_0 = \frac{\tau_c}{\rho g}\frac{2\cos(\arctan\mu_s)}{\cos\alpha\sin(\alpha-\arctan\mu_s)}.$$

This height is minimal, equal to H_c, when the angle of rupture is given by the Mohr–Coulomb failure criterion on the Mohr circle [13],

$$\alpha = \frac{\arctan(\mu_s)}{2} + \frac{\pi}{4}. \tag{5}$$

For example, with $\mu_s = 0.3$, the column must exceed about $5\,\ell_c$ to flow. Although this length controls the granular macroscopic cohesion from a continuum point of view, it is not well defined at the grain scale. In the following, we attempt to bridge the gap by relating its value to the discrete contact forces.

To do so, we first test this threshold with the continuous approach (Sec. II) and then with the contact dynamics simulations (Sec. III). Finally, we compare them and discuss the relation between the material and the grain-scale cohesion (Sec. IV).

II. CONTINUOUS APPROACH

A. Rheology

We describe here our continuous approach to model cohesion in the granular material. As mentioned in the Introduction, we consider the granular column as a fluid of a peculiar rheology, namely, a dry granular material supplemented by a yield stress [Eq. (2)].

For dry granular materials, the so-called $\mu(I)$-rheology is commonly used to model dense flows. This rheology takes into account the granular threshold to initiate the flow and involves a complex dependence on the shear rate, encapsulated by the inertial number [8,14],

$$I = \frac{\dot\gamma d}{\sqrt{P/\rho}}. \tag{6}$$

We defined $\dot\gamma = \sqrt{2}D_2$, where $D_2 = \sqrt{\mathbf{D}:\mathbf{D}}$ is the second invariant of the rate of strain tensor $\mathbf{D}$, P the pressure, and d and ρ are the diameter and density of the grain, respectively.

Then, the friction coefficient evolves as the following function of I:

$$\mu(I) = \mu_s + \frac{\Delta\mu}{I_0/I + 1}, \tag{7}$$

where μ_s is the static friction coefficient, $\Delta\mu$ is the difference between the dynamic and static friction coefficient, and I_0 is an initial inertial number. This rheology, first introduced by MiDi [8] for stationary flows, was shown to be valid in the intricate flow configuration of dry granular collapse by Lacaze and Kerwell [10] and implemented successfully in continuum models [6,7,15,16] since Lagrée *et al.* [5].

Now, to account for the cohesion, we supplement this rheology by a yield stress τ_c, which is classically used for viscoplastic fluids such as Bingham fluids. This threshold, on the contrary to the granular one, does not depend on the pressure. Overall, this peculiar rheology for our cohesive granular material translates in a relation between shear stress and pressure,

$$|\boldsymbol{\tau}| = \mu(I)P + \tau_c. \tag{8}$$

More generally, we assume that the internal stress tensor follows

$$\boldsymbol{\sigma} = -P\mathbf{I} + 2\eta\mathbf{D}, \quad \text{with } \eta = \frac{\tau_c + \mu P}{\sqrt{2}D_2}, \tag{9}$$

where η is an effective viscosity.

This rheology assumes that frictional properties, described by the term $\mu(I)$ are independent of cohesive properties, encapsulated by τ_c only. This may not be the case, in general, where, for example, μ_s could vary with cohesion [4,17] and grain stiffness [18]. Also, it has been shown that cohesion decreases with inertial number [19]. Here, as we focus the study on the initiation of the granular motion, and for lack of a comprehensive theory, we decide not to take these effects into account in the following.

In our simulations, we start by using the values of Jop *et al.* [9] for the static coefficient $\mu_s = 0.38$, $\Delta\mu = 0.26$, and $I_0 = 0.279$. We also fix the grain size such that we have 30 grains in a column width ($d = R_0/30$, with R_0 the width of the column). However, this grain size does not have a physical meaning in our description.

B. Numerical implementation and parameters

We now solve the Navier–Stokes equations for this fluid using the flow solver Basilisk, which is based on a projection method and a volume-of-fluid approach [5,20]. Thus, we define two phases: the granular column and its surrounding air. The properties of the surrounding air does not affect the column dynamics provided that its viscosity and density are small enough compared to the column's ones [5].

This solver uses an adaptive mesh refinement method [21]. Thus, we maximally refine the grid in the column and

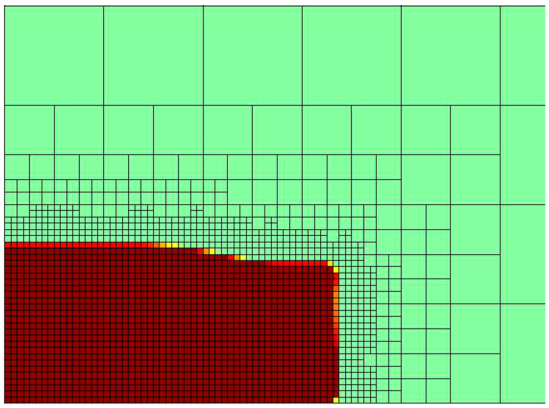

FIG. 2. Adaptive mesh refinement during a simulation of the collapse of a cohesive granular column (continuous approach). The color indicates the phase of the fluid. In red (or dark area): cohesive granular material. In green (or light area): surrounding air.

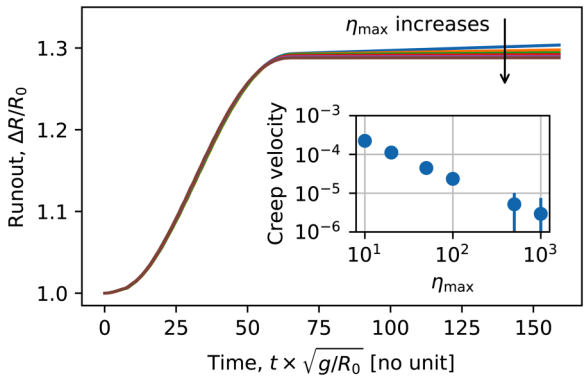

FIG. 3. Runout of the column as a function of time, for different regularization viscosity (continuous approach) η_{max} (with $\ell_c/H_0 = 0.1$). Inset: Final velocity of the material against the boundary viscosity η_{max}.

decrease its size in the surrounding fluid, which optimizes the time of computation (Fig. 2). In the computation, equations are solved using non-dimensional variables (Table I).

According to the rheology, the fluid then flows with an effective viscosity. However, as granular matter must stop when its viscosity diverges, we thus regularize its motion by introducing a maximum viscosity, η_{max}. As a result, the column freezes and slowly creeps at the end of the simulation. We then have the following expression for the viscous stress and the effective viscosity [5]:

$$\boldsymbol{\tau} = 2\eta\mathbf{D}, \quad \text{where } \eta = \min\left(\frac{\tau_c + \mu(I)P}{\sqrt{2}D_2}, \eta_{max}\right). \tag{10}$$

There is not a unique manner to regularize the viscosity [15,22], but we chose the simplest one by limiting the viscosity with a maximum, as did Lagrée *et al.* [5]. They found that, for dry granular material, the values of η_{max} does not affect the final shape of the deposit as long as it is larger than 100.

We checked this dependency for our cohesive material by measuring the creeping velocity of the front, when it reached its final shape, and thus after typically $t = 5\sqrt{R_0/g}$. We observe that for η_{max} of above 100, this variation remains smaller than about $10^{-5}R_0$, which we find to be negligible (Fig. 3).

C. Simulations

We now show a first example for the slumping of a granular column with $\eta_{max} = 100$ (Fig. 4). In this example, we fix the domain size to $L_D = 10$ and chose $H_0 = 1$ and $R_0 = 2$ for the initial geometry of the column. At its maximum, the grid size is then $L_D/2^8$. We take the cohesive length equal to $\ell_c/H_0 = 0.1$, which remains small compared to the height of the column; the column thus releases and flows.

By plotting the intensity of the inertial number I, we observe that a band appears, where the shear rate is maximum. In the corner above this band, the shear remains negligible such that the corner does not deform and is almost undisturbed in the final shape. The final runout of the collapse, defined as the maximum distance traveled by the front of the flow, is then smaller than that of a cohesionless column.

This band makes an angle α with the horizontal. We expect that this angle is a function of the friction coefficient, through Eq. (5).

To measure this angle properly, we detect where the material moved from $10^{-2}\sqrt{gR_0}$ (dashed line, Fig. 4). Although this trend is well reproducible for a cohesionless granular material, it is not the case for a cohesive one (Fig. 5). In particular, the theory systematically overestimates it. This may come from the uncertainty in the detection of the angle, which requires a local threshold criterion. Overall, as the trend is smooth, the angle has the good order of magnitude, and we will see that it does not affect the threshold of slumping, on which we focus in the following.

TABLE I. Parameters used for the dimensional analysis.

Width	Pressure	Velocity	Time
R_0	$\rho g\, R_0$	$\sqrt{gR_0}$	$\sqrt{R_0/g}$

D. Stability of the column

We now perform a series of simulations where we vary the height of the column and the yield stress, and thus the cohesion length ℓ_c.

First, we fix a small cohesion in the granular bulk ($\ell_c/R_0 = 0.1$) and vary the column's height (vertical line in Fig. 6). If the column is high enough, it releases, then flows and acquires a stationary shape after approximately $t = 5\sqrt{R_0/g}$. Conversely, if the height is too small, the column does not flow and is cohesive enough to remain in its initial shape. This threshold follows Eq. (3) for a given cohesion.

Then, we keep the height constant, and vary the cohesion of the granular material ℓ_c (horizontal line in Fig. 6). Still, the column releases for a low cohesion, and it exists a threshold above which cohesion forces are sufficient to keep the column stable.

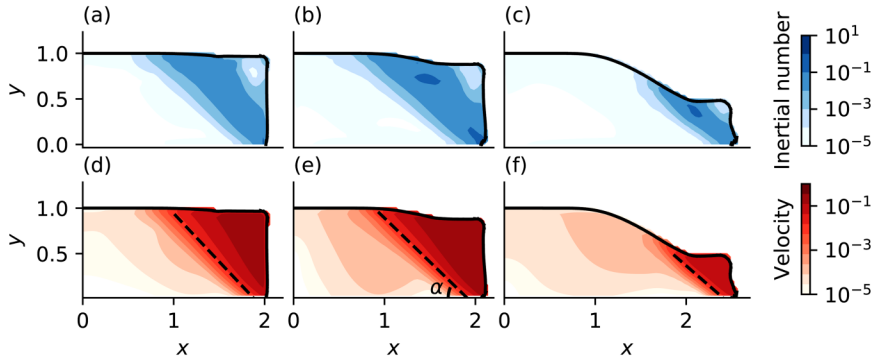

FIG. 4. Slumping of the cohesive granular column (continuous approach) with time. The colorbar indicates the intensity of the velocity. (a) and (d) $t = 0$; (b) and (e) $t = 1.5\sqrt{R_0/g}$; (c) and (f) $t = 3\sqrt{R_0/g}$ (final shape).

On the same figure, we plot the theoretical threshold given by Eq. (3), which provides a good agreement, without any fitting parameter (dashed line, Fig. 6). This limit validates the implementation of cohesion in the granular column for small to moderate cohesion lengths.

Furthermore, we will prefer to use the grain diameter d to compare our results with the discrete approach, which we do in Sec. III.

III. DISCRETE APPROACH

A. Contact dynamics simulations

The cohesive granular matter is simulated applying the contact dynamics (CD) algorithm [11,12,23], already applied for column collapse problems in [5,24,25]. The basic ingredients of this method are Coulombic solid friction and hardcore repulsion. Solid friction imposes locally that the normal contact force f_n and tangential contact forces f_t satisfy $f_t \leq \mu_c f_n$, where μ_c is the coefficient of friction at contact, while hardcore repulsion ensures that the values of normal forces computed are such that the overlap characterizing the existence of contacts remains as small as possible. In the case of noncohesive material, forces at contacts are exclusively compressive; in the cohesive case, forces in extension are allowed. This implies the introduction of a contact adhesive force F_{adh} that imposes the maximum value attainable by a force in extension before the contact is disrupted and opens. Based on the literature [26,27], we set the value of F_{adh} proportional to a granular Bond number and the mean weight of the grains involved in the contact,

$$F_{adh} = -B_{ond} m_{ij} g, \tag{11}$$

with $m_{ij} = \left(2/m_i + 2/m_j\right)^{-1}$ and i and j are the two grains involved. Its value is systematically changed and its influence analyzed in Subsection IV.

The contact friction μ_c was set to 0.5 and its value/influence was not investigated nor discussed here. We may just make clear that the friction forces are computed for the normal forces without any cohesive contribution. Moreover, a coefficient of restitution e set the amount of energy dissipated in collisions. Its value was set to $e = 0.1$ (namely, rather inelastic) and not varied.

B. Numerical setup

The systems simulated in this contribution are columns in 2D, as shown in Fig. 7. The columns are made of circular beads of mean diameter $d = 0.005$ m, uniformly distributed in the range [0.004, 0.006] to avoid geometrical ordering that may strongly dominate the failure and stability of the granular construction. The column are prepared by random rain in containers with initially a zero cohesion to ensure a volume fraction, or compacity, such as expected in a random packing with this size disparity; we obtain $\phi = 0.85 \pm 0.03$. Once

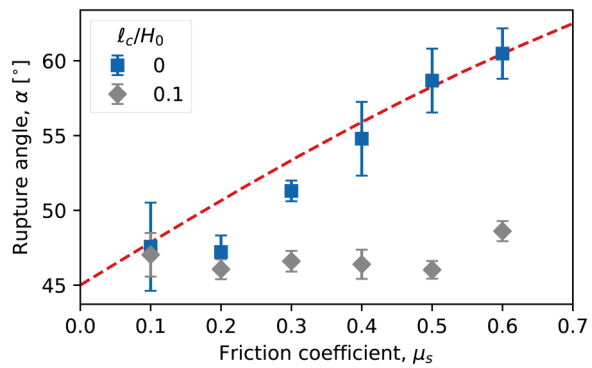

FIG. 5. Rupture angle as a function of the friction coefficient (continuous approach). Dashed red line: Mohr–Coulomb theory [Eq. (5)]. Blue square markers: for granular columns without cohesion. Grey diamond markers: for cohesive columns, with a cohesion length of $\ell_c/H_0 = 0.1$.

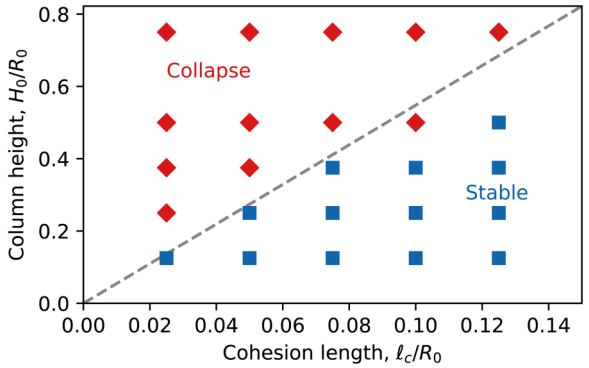

FIG. 6. Stability map. Gray dashed line: analytical limit [Eq. (3)]. Points : numerical simulations with Basilisk (continuous approach). Blue square markers: the pile is stable and never collapses. Red diamond markers: the column collapses.

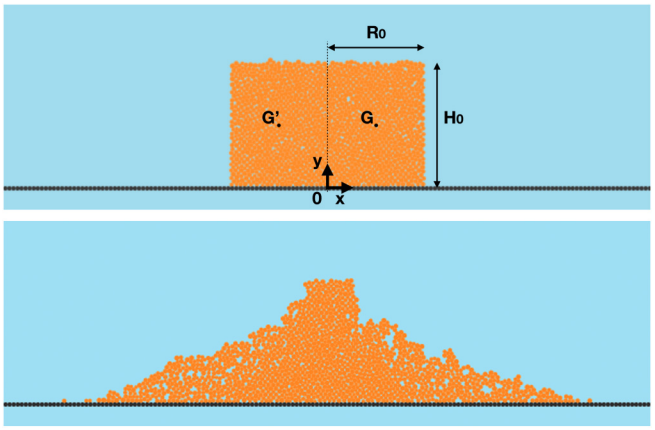

FIG. 7. An example of the discrete collapse of a cohesive column with the initial state (top) and the final state (bottom). The number of grains is 1500; the B_{ond} number is 100.

the packing has reached his final equilibrium state, a last series of computation time steps with $B_{ond} \neq 0$ are performed; this ensures that the initial condition for slumping (once the container walls are no longer there) is compatible with cohesion and the first few time steps of the computations do not see grains losing equilibrium because contact open before computation may restore their viability through cohesion. We should recall here that DC does not rely on an explicit formulation of the cohesive contact law using very small time steps but on a nonsmooth condition requiring going through an implicit iteration.

The dimension of both columns, namely, initial height H_0 and initial width R_0, changed. The intensity of the contact cohesive threshold is also systematically varied [through varying the B_{ond} number, Eq. (11) in Sec. IV]. We essentially performed three series of simulations, with dimensions, number of grains, and cohesive threshold (B_{ond} number), all independently varied; a summary of the values adopted is given in Table II B. Considering these values, the behavior obtained in each series varies from collapse with spreading of most of the materials to slumping of part of the material following a well-defined failure zone, to equilibrium/stability with slow creeping. Figure 8 shows these three occurrences for a B_{ond} number of successively 50, 100, and 150.

C. Evaluating the equilibrium of the discrete columns

We need a criteria to decide whether a column is stable or unstable. Although this may sound an obvious thing to do, discrete columns do not always fall clearly into one category or the other, but might simply lose a small part of an edge, or see only few grains rolling down while the rest of the pile remains static, or see one angle perfectly static while the other loses equilibrium. In order to define a criterion for the stability of the column, we simply quantify the slumping as the relative distance traveled by the secondary centers of mass G and G' (i.e., centers of mass of each half of the initial column) following both axis, namely, vertical slumping and horizontal outspread, computing

$$\Delta X = \frac{|x_{(G,\infty)} - x_{(G,0)}|}{|x_{(G,0)}|}, \tag{12}$$

$$\Delta Y = \frac{|y_{(G,\infty)} - y_{(G,0)}|}{y_{(G,0)}}, \tag{13}$$

where $x_{(G,0)}$, $x_{(G,\infty)}$, $y_{(G,0)}$, and $y_{(G,\infty)}$ (respectively, $x_{(G',0)}$, $x_{(G',\infty)}$, $y_{(G',0)}$, and $y_{(G',\infty)}$) are the initial and final coordinates of the secondary center of mass G (respectively, G'). For each simulation, ΔX and ΔY are computed for both secondary centers of mass G and G' and then simply averaged. The vertical slump ΔY is plotted as a function of the horizontal outspread ΔX in log-log coordinates for all simulations, from Table II B, in Fig. 9. We obtain two very distinct clouds of points for stable and unstable columns, joined by a handful of more uncertain realizations where only few grains roll down, creating a more ambiguous group closing the gap between two clear well-separated clouds of points. Nevertheless, these points are distinct enough to be distributed to one group or the other so that we can now map out a stability graph plotting for each group, namely, stable or unstable, the initial height H_0 (normalized by d) as a function of the B_{ond} number, and compare it with the theoretical prediction (3), and with continuum simulations.

Using this criteria, we determine the behavior (stable or not) of all simulations presented in Table II B. The result is displayed in Fig. 10, where two well-defined spaces for stable or unstable (H_0, B_{ond}) pairs come out. From visual inspection, the linear dependence $H_0/d = 0.45B_{ond}$ forms a satisfactory boundary between both states, defining a discrete yielding height.

We can now compare the discrete granular failure behavior with the continuous one.

IV. STABILITY ANALYSIS OF DISCRETE AND CONTINUUM COLUMNS

A. Comparing continuum and discrete approaches

As reminded above, the stability of a continuum cohesive column of rheology $\tau = \tau_c + \mu(I)P$ requires that the height

TABLE II. Table of discrete simulations performed.

Simulations series	Initial height, H_0	Initial width, R_0	Initial aspect ratio, a	Number of grains	Cohesion number, B_{ond}
simu A (I)	31 d	[10d; 42d]	[0.72, 3.06]	[580, 2500]	[0, 200]
simu B (H)	[10d, 46 d]	[10d, 46d]	1.00 ± 0.02	[186, 4228]	[0, 250]
simu C (G)	[6d, 43 d]	16d	[0.377, 2.667]	[153, 1326]	[0, 200]

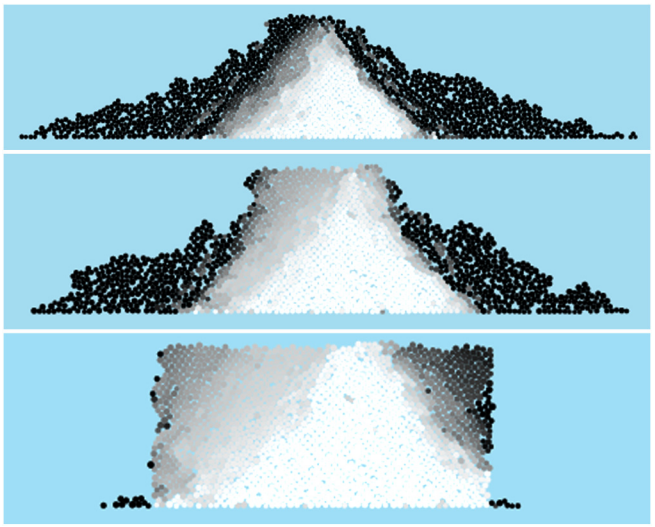

FIG. 8. An example of the final slumping of a discrete cohesive column with a B_{ond} number of 50, 100, and 150 (top to bottom). In black are particles whose total displacement is greater than $5d$; the gray scale for the other grains is linear in cumulative displacement.

of the wedge remains below the yield value H_c defined by Eq. (3). This threshold height, however, depends on the term τ_c referring to the macroscopic cohesion, or yield stress, valid over any representative volume of the continuum, at any rate valid for a whole column or wedge. No such quantity is readily available for the discrete counterpart of a cohesive column; indeed, the sole fully controlled ingredient in the discrete method is the cohesive contact force, namely, hardly a quantity that one may identify with a "macroscopic cohesion." The effective macroscopic cohesion of a granular packing will of course reflect the intensity of contact forces at first order, but not only. The orientation of the contacts, the volume fraction of the system, and microtextural aspect such as particle shape will certainly play a role, as discussed in [28,29]. Meanwhile, determining computationally a quantity equivalent to τ_c would require a systematic analysis of the stress tensor for well-defined configurations (such as shear cells), and this for steady flows so that the friction could be unambiguously computed. This is hardly feasible in the transient complex dynamics studied here. Hence, in a first step, we will stick to the contact cohesion F_{adh} and discuss how to relate the B_{ond} number to the macroscopic yield stress τ_c.

The definition of F_{adh} as used locally for each contact of the discrete systems in the CD simulations is given by

$$F_{adh} = -B_{ond} :m_p g. \tag{14}$$

In the following, we consider the mean contact adhesive force, replacing the weight of the two grains precisely in contact m_{ij} by the mean particle weight $m_p = \pi d^2/4$, with d being the mean grains diameter: In order to compare quantitatively the behavior of discrete slumping collapses with their continuum counterparts, we *a priori* define a macroscopic cohesive stress representative for the granular packing simulated with the mean contact cohesive force F_{adh}. Therefore, we introduce a characteristic length L, which we assume to be the macro-/mesoscale over which cohesive stress applies,

$$\frac{|F_{adh}|}{L} = \frac{B_{ond}}{L}\frac{\pi d^2}{4}\rho g, \tag{15}$$

which, if we write $\tau_c \simeq F_{adh}/L$, gives

$$\frac{\tau_c}{\rho g} = \frac{\pi d^2}{4L} \times B_{ond}. \tag{16}$$

The characteristic length L is unknown; we may only guess that it probably is greater than a grain diameter (the smallest length scale in the system if we omit the explicit description of contacts) and of the order of few grain diameters by analogy with the often besought force chains. These

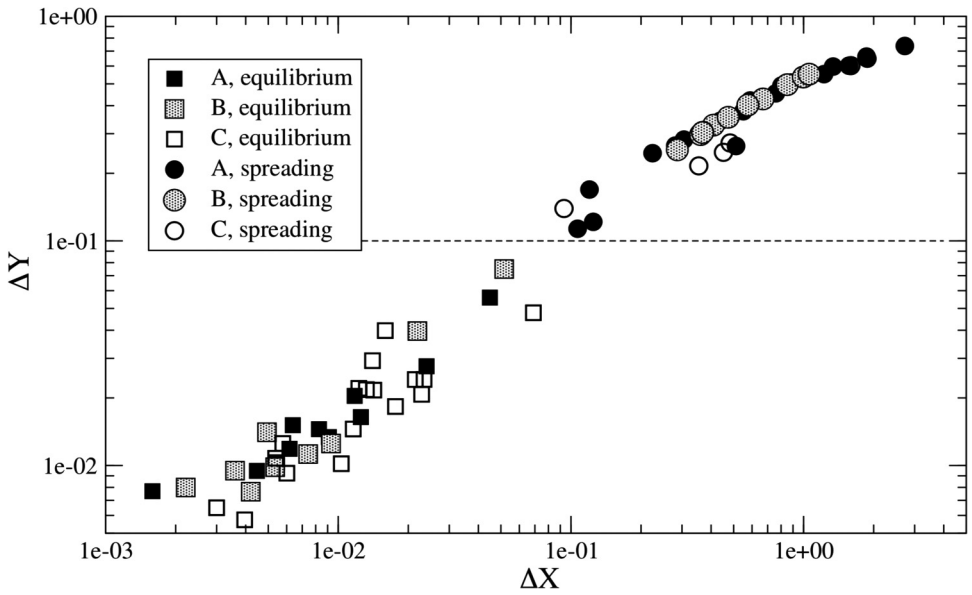

FIG. 9. Vertical slumping ΔY against horizontal outspread ΔX for all discrete simulations. We chose the value $\Delta Y = 0.1$ to distinguish columns at equilibrium (□ symbols) from those slumping (○ symbols), although there are few simulations who do gather around this value. The gray scale for the three series of simulations A, B, C is presented in Table II B.

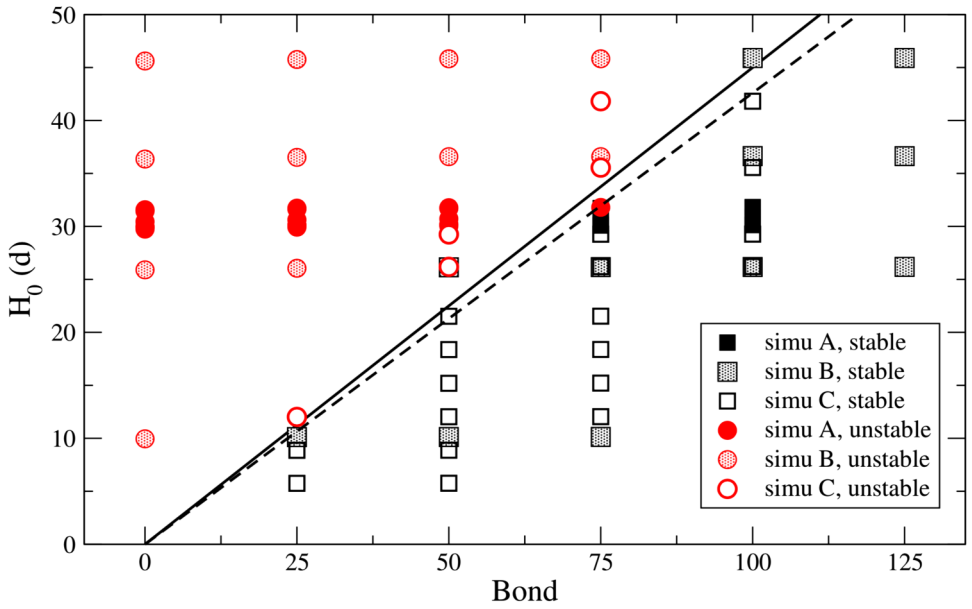

FIG. 10. Initial height H_0 (normalized by d) as a function of the B_{ond} number for the three series of discrete simulations A, B, C is presented in Table II B. The full line which divides stable columns (□ symbols) and unstable ones (◯ symbols) verifies $H_0/d = 0.45B_{ond}$. The dotted line shows the favorable case of the "Rumpf–Richefeu" prediction [28] (Sec. IV C) with $\mu = 0.3$ [Eq. (20)].

are, however, if reasonable, yet only guesses, which ignore the fundamental role of the granular fabric when trying to model the mean mechanical properties of a granular sample. In the absence of a clear idea, we will merely assume that $L = nd$, where n would be the typical number of grains onto which macroscopic cohesive stress builds up, and we will derive its value from the stability analysis of the simulated discrete columns shown in Fig. 11.

The latter shows that the linear dependence $H_0/d = 0.45B_{ond}$ forms a satisfactory boundary between both states, defining a discrete yielding height that can be confronted with prediction (3). We can rewrite (3) using (16) so that

$$\frac{H_c}{d} = \frac{\pi}{\sqrt{\mu_s^2 + 1} - \mu_s} \times \frac{1}{n} \times B_{ond}, \tag{17}$$

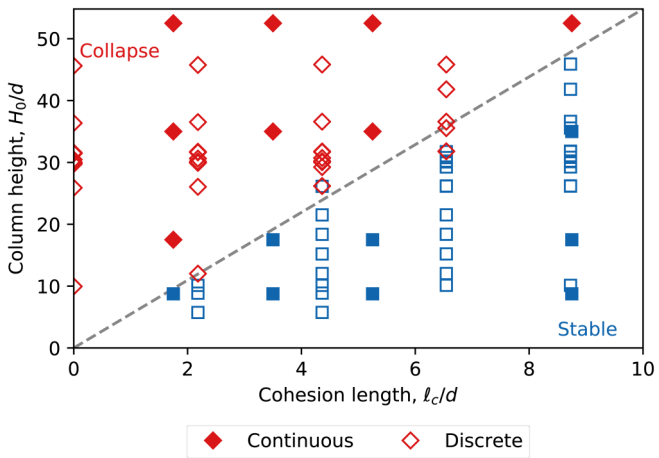

FIG. 11. Stability map with discrete and continuous data. Filled symbols: continuous simulations with Basilisk. Empty symbols: discrete simulations with contact dynamics. Gray dashed line: analytical limit [Eq. (3)]. Blue square markers: the pile is stable and never collapses. Red diamond markers: collapse of the granular pile occurs.

where μ_s is the macroscopic friction, whose value for our systems is unknown. Considering that the contact friction is $\mu_c = 0.5$, a reasonable estimate is $\mu_s = 0.3$ [30], which leads readily to $H_c/d = 4.22/n \times B_{ond}$, which gives $n = 9$, namely, $L = 9d$, which seems a reasonable value. Note that assuming $\mu_s = 0.5$ leads to $L = 11d$ so that the result is poorly depending on the details of the friction coefficient (whose value remains generally bounded in a small interval) [30].

B. Comparing discrete and continuum

From the analysis above, we found that the stability analysis based on Mohr–Coulomb applies to discrete piles providing the cohesive stress is determined over a characteristic length of $L = 9d$. Injecting this result in Eq. (16) gives

$$\frac{\ell_c}{d} = \frac{\pi}{36} B_{ond},$$

which we can use to plot on a single graph both discrete and continuum data points for stable and unstable piles. Note that the grain diameter, in continuum simulations, plays a role only through the rheological model which accounts for the dependence on the inertial number I, inducing the frictional properties to vary with d. Verifying that this dependence is very small (since the I-dependence is virtually nil at the onset of the failure), we neglected it and varied d in order to allow the normalized height H_0/d for continuum piles to fall in the same interval as for discrete piles. Doing so, we can map discrete and continuum simulations onto a single final graph in Fig. 11.

C. Discussion

Alternatively, we can adapt the analysis developed by Richefeu *et al.* [28] from the Rumpf equation [29] for 3D wet granular media, merely modifying it for 2D dry quasi-

monodisperse systems, and using expression (14) for contact cohesive forces F_{adh} rather than capillary forces. Following [28], the density of cohesive contacts is given by half the mean number of cohesive contacts per particle Z_c divided by the free volume in 2D, i.e., the mean volume of a Voronoi cell surrounding the particle, i.e., the average particle volume $V_p = \pi d^2/4$ divided by the solid fraction ϕ. Considering the cohesive forces to be $F_{adh} = mgB_{ond} = \rho g V_p B_{ond}$, we obtain for the theoretical tensile strength for an assembly of cohesive particles,

$$\sigma_c = \frac{d}{4}\phi Z_c \times \rho g \times B_{ond}, \tag{18}$$

with ϕ being the packing volume fraction and Z_c being the mean number of cohesive contacts per particle. Hence, the theoretical cohesion $\tau_c = \mu_s \sigma_c$ readily gives

$$\frac{\tau_c}{\rho g} = \frac{d}{4}\mu_s \phi Z_c \times B_{ond}. \tag{19}$$

Replacing theoretical expression (19) in the theoretical stability condition (3), we obtain

$$\frac{H_c}{d} = \frac{\mu_s}{\sqrt{\mu_s^2 + 1} - \mu_s} \times \phi Z_c \times B_{ond}, \tag{20}$$

which we can confront to the stability graph (Fig. 10).We, therefore, need to evaluate Z_c; in Richefeu *et al.* [28], Z_c (the number of capillary bounds in 3D) is assumed to be 6. In our system, Z_c is simply the mean number of contacts bearing negative forces per grain; its value for a 2D system counting 4228 grains with $B_{ond} = 125$ is $Z_c = 1.3$ (the mean number of contacts irrespective of the force transmitted is between 3 and 3.5). Taking $\phi = 0.82$ (as measured), and assuming $\mu = 0.3$, prediction (20) yields $H_c/d = 0.426 B_{ond}$, in good agreement with what is observed from numerical simulations (Fig. 10). However, the result is sensitive to the value of μ chosen; taking $\mu = 0.5$ leads to $H_c/d = 0.86 B_{ond}$, in a much lesser agreement with observations.

More to the point, prediction (20) is very dependent on the value taken by ϕ and Z_c; a rapid inspection of the simulations shows that both quantities are dependent on the B_{ond} number. For simulations taken from series B [Table II B], we find that ϕ varies between 0.78 (for $B_{ond} = 100$) and 0.82 (for $B_{ond} = 125$), namely, a modest 5% variations; but the mean number of cohesive contacts per particle varies between 0.75 (for $B_{ond} = 50$) and 1.3 (for $B_{ond} = 125$), creating alone a 40% uncertainty in expression (20) (see Fig. 12). A dedicated work would be needed to clarify this aspect.

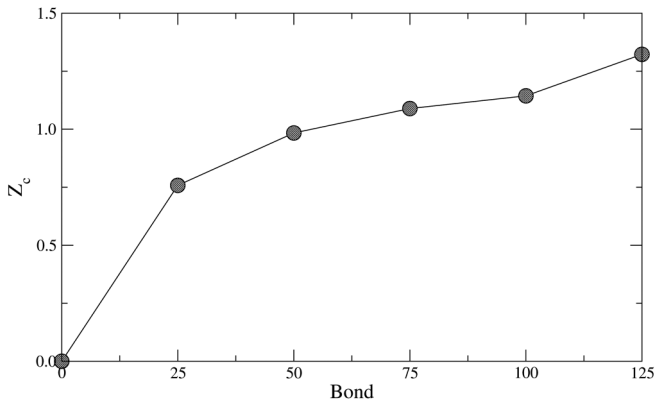

FIG. 12. Mean number of cohesive contacts (i.e., mean number of contacts bearing negative forces) per particle Z_c as a function of the normalized cohesive force $B_{ond} = F_{adh}/mg$ for simulations from series B [Table II B], with $R_0 = H_0 = 46$ d, counting 4228 grains.

V. CONCLUSION

In this article, we investigated how cohesion influences the release of a granular column. We first developed a code where we solve Navier–Stokes equation with a VOF solver (Basilisk). We checked this code by investigating the threshold height over which a column flows or not. We found good agreement with the Mohr–Coulomb criterion, which predicts this threshold, without any fitting parameter.

We then compared this approach with a code of contact dynamics, which models the dynamics of the column at the grain scale. By comparing the height threshold, we link cohesion forces at the grain scale with the macroscopic cohesive length, and thus the yield stress, as follows:

$$\frac{\ell_c}{d} = (0.087 \pm 0.005) B_{ond}, \tag{21}$$

for the given granular material simulated. This prefactor, however, depends on the grain-scale parameters used in our contact-dynamics algorithm, as the contact friction, or the grain-size distribution. Thus, we estimated this relationship in the light of the work of Rumpf–Richefeu, which provides an expression for the macroscopic cohesive length, as a function of the number of cohesive contacts, the compacity, and the friction coefficient

$$\frac{\ell_c}{d} = \frac{\mu_s \phi Z_c}{4} B_{ond}. \tag{22}$$

We measured Z_c and ϕ in our contact dynamics simulations and calculated the friction coefficient based on the contact friction coefficient. This expression thus yields a coefficient of 0.08 ± 0.01, which is in good agreement with our simulations.

Now that cohesion is numerically validated for the stability threshold of a column, much remains to be done to understand how cohesion alters the dynamics of the collapse and the final shape of the deposit. To do so, we will likely need to compare numerics with experiments. Ideally, experiments would be conducted with a controlled-cohesive granular material, recently developed by Gans *et al.* [4]. This would provide new insights into the flow properties of a cohesive material and, hopefully, on the concept of "flowability."

ACKNOWLEDGMENTS

This work is part of the COPRINT Project (http://coprint226940055.wordpress.com) supported by the ANR Grant No. ANR-17-CE08- 0017.

REFERENCES

[1] Iverson, R. M., "Landslide triggering by rain infiltration," Water Resour. Res. **36**, 1897–1910, https://doi.org/10.1029/2000WR900090 (2000).

[2] Castellanos, A., "The relationship between attractive interparticle forces and bulk behaviour in dry and uncharged fine powders," Adv. Phys. **54**, 263–376 (2005).

[3] Bocquet, L., E. Charlaix, and F. Restagno, "Physics of humid granular media," C. R. Phys. **3**, 207–215 (2002).

[4] Gans, A., O. Pouliquen, and M. Nicolas, "Cohesion-controlled granular material," Phys. Rev. E **101**, 032904 (2020).

[5] Lagrée, P.-Y., L. Staron, and S. Popinet, "The granular column collapse as a continuum: Validity of a two-dimensional Navier-Stokes model with a μ(i)-rheology," J. Fluid Mech. **686**, 378–408 (2011).

[6] Staron, L., P.-Y. Lagrée, and S. Popinet, "The granular silo as a continuum plastic flow: The hour-glass vs the clepsydra," Phys. Fluids **24**, 103301 (2012).

[7] Staron, L., P.-Y. Lagrée, and S. Popinet, "Continuum simulation of the discharge of the granular silo," Eur. Phys. J. E **37**, 5 (2014).

[8] MiDi, G., "On dense granular flows," Eur. Phys. J. E **14**, 341–365 (2004).

[9] Jop, P., Y. Forterre, and O. Pouliquen, "A constitutive law for dense granular flows," Nature **441**, 727–730 (2006).

[10] Lacaze, L., and R. R. Kerswell, "Axisymmetric granular collapse: A transient 3D flow test of viscoplasticity," Phys. Rev. Lett. **102**, 108305 (2009).

[11] Jean, M., and J. J. Moreau, "Unilaterality and dry friction in the dynamics of rigid body collections," Proc. Contact Mechanics Int. Symp., Edt. A. Cu ier, PPUR, 31 8 (1992).

[12] Moreau, J. J., "Sorne numerical methods in multibody dynamics: Application to granular materials," Eur. J. Mech. A/Solids **13**, 93–114 (1994).

[13] Nedderman, R. M., *Statics and Kinematics of Granular Materials* (Cambridge University Press, Cambridge, 2005).

[14] Da Cruz, F., S. Emam, M. Prochnow, J.-N. Roux, and F. Chevoir, "Rheophysics of dense granular materials: Discrete simulation of plane shear flows," Phys. Rev. E **72**, 021309 (2005).

[15] Chauchat, J., and M. Médale, "A three-dimensional numerical model for dense granular flows based on the μ (i) rheology," J. Comput. Phys. **256**, 696–712 (2014).

[16] Dunatunga, S., and K. Kamrin, "Continuum modelling and simulation of granular flows through their many phases," J. Fluid Mech. **779**, 483–513 (2015).

[17] Roy, S., S. Luding, and T. Weinhart, "A general (ized) local rheology for wet granular materials," New J. Phys. **19**, 043014 (2017).

[18] Mandal, S., M. Nicolas, and O. Pouliquen, "Insights into the rheology of cohesive granular media," Proc. Natl. Acad. Sci. U.S.A. **117**, 8366–8373 (2020).

[19] Berger, N., E. Azéma, J.-F. Douce, and F. Radjai, "Scaling behaviour of cohesive granular flows," Europhys. Lett. **112**, 64004 (2016).

[20] Scardovelli, R., and S. Zaleski, "Direct numerical simulation of free-surface and interfacial flow," Annu. Rev. Fluid Mech. **31**, 567–603 (1999).

[21] Popinet, S., "Gerris: A tree-based adaptive solver for the incompressible euler equations in complex geometries," J. Comput. Phys. **190**, 572–600 (2003).

[22] Frigaard, I., and C. Nouar, "On the usage of viscosity regularisation methods for visco-plastic fluid flow computation," J. Nonnewton. Fluid Mech. **127**, 1–26 (2005).

[23] Radjai, F., M. Jean, J.-J. Moreau, and S. Roux, "Force distributions in dense two-dimensional granular systems," Phys. Rev. Lett. **77**, 274–277 (1996).

[24] Staron, L., and E. Hinch, "Study of the collapse of granular columns using dem numerical simulation," J. Fluid Mech. **545**, 1–27 (2005).

[25] Staron, L., and E. Hinch, "The spreading of a granular mass: Role of grain properties and initial conditions," Granular Matter **9**, 205 (2007).

[26] Nase, S. T., W. L. Vargas, A. A. Abatan, and J. McCarthy, "Discrete characterization tools for cohesive granular material," Powder Technol. **116**, 214–223 (2001).

[27] Rognon, P. G., J.-N. Roux, M. Naaim, and F. Chevoir, "Dense flows of cohesive granular materials," J. Fluid Mech. **596**, 21–47 (2008).

[28] Richefeu, V., M. S. El Youssoufi, and F. Radjai, "Shear strength properties of wet granular materials," Phys. Rev. E **73**, 051304 (2006).

[29] Rumpf, H., "Zur theorie der zugfestigkeit von agglomeraten bei kraftuebertragung an kontaktpunkten," Chem. Ing. Tech. **42**, 538–540 (1970).

[30] Staron, L. H., "Etude numérique des mécanismes de déstabilisation des pentes granulaires," Ph.D. thesis, Institut de physique du globe, Paris, 2002.